# Enhanced biobased carbon materials made from softwood bark via a steam explosion preprocessing step for reactive orange 16 dye adsorption

Andreas Averheim [a], Glaydson Simões dos Reis [b], Alejandro Grimm [b], Davide Bergna [c], Anne Heponiemi [c], Ulla Lassi [c], Mikael Thyrel [b,*]

[a] *Valmet AB, Fiber Technology Center, SE-851 94 Sundsvall, Sweden*
[b] *Swedish University of Agricultural Sciences, Department of Forest Biomaterials and Technology, SE-901 83 Umeå, Sweden*
[c] *University of Oulu, Research Unit of Sustainable Chemistry, FI-90570 Oulu, Finland*

## HIGHLIGHTS

- A novel process for active carbon using steam explosion preconditioning is presented.
- Steam explosion prior to activation improves carbon surface area and functionality.
- Maximum adsorption (218 mg g$^{-1}$) was obtained using steam-exploded material.
- Steam exploded materials showed higher efficiencies in synthetic effluent dye removal.
- The large surface area of carbons supports pore-filling as main adsorption mechanism.

## ARTICLE INFO

## ABSTRACT

The growing textile industry produces large volumes of hazardous wastewater containing dyes, which stresses the need for cheap, efficient adsorbing technologies. This study investigates a novel preprocessing method for producing activated carbons from abundantly available softwood bark. The preprocessing involved a continuous steam explosion preconditioning step, chemical activation with $ZnCl_2$, pyrolysis at 600 and 800 °C, and washing. The activated carbons were subsequently characterized by SEM, XPS, Raman and FTIR prior to evaluation for their effectiveness in adsorbing reactive orange 16 and two synthetic dyehouse effluents. Results showed that the steam-exploded carbon, pyrolyzed at 600 °C, obtained the highest BET specific surface area (1308 m$^2$/g), the best Langmuir maximum adsorption of reactive orange 16 (218 mg g$^{-1}$) and synthetic dyehouse effluents (>70 % removal) of the tested carbons. Finally, steam explosion preconditioning could open up new and potentially more sustainable process routes for producing functionalized active carbons.

## 1. Introduction

Biobased carbon materials have been researched intensively in recent years for the potential use in, for example, supercapacitors (Correa & Kruse, 2018; Wang et al., 2020), batteries (Correa & Kruse, 2018; Zhang et al., 2015), adsorbents (Bilal et al., 2022; Praveen et al., 2022; Qasem et al., 2021), and catalysts (Correa & Kruse, 2018). Biomass has the potential to replace fossil-based precursors such as coal or graphite for these applications and, in addition, provide improved properties or new functionalities that may increase the final product's performance.

Biobased adsorbents have been used by humanity for thousands of years and cover a wide range of materials that can be used to purify gases or liquids (Dąbrowski, 2001). Biomass sources such as low-cost byproducts from agriculture or industry are of particular interest as precursors as these may provide cost-efficient and sustainable materials. A wide range of agricultural residues has been investigated in literature as raw materials for adsorbent production (Ioannidou & Zabaniotou, 2007), for example, corn straw, rice straw, wheat straw, bagasse, corn stover, and cotton residues together with industrial residues such as

spruce bark (dos Reis et al., 2021b), and sludges (Won et al., 2006) to mention a few. The wide range of potential raw materials and choices for processing also gives rise to a wide selection of adsorbent materials that could be produced for tailor-made purposes.

A large surface area is a typical characteristic of biochars used as adsorbents due to their meso- and microporous structure (Dąbrowski, 2001), which can be achieved through one or several physical, thermal and chemical treatment steps (Bilal et al., 2022; Correa & Kruse, 2018; Praveen et al., 2022). Thermal conversion processes, such as pyrolysis, hydrothermal carbonization (HTC), or gasification, are often involved in producing biochar (Praveen et al., 2022), while activation steps could be incorporated in the process such as physical activation by steam or $CO_2$, or chemical activation with chemicals such as $H_3PO_4$, $K_2CO_3$, KOH or $ZnCl_2$ to obtain an activated carbon (AC) (Bilal et al., 2022; Correa & Kruse, 2018). The materials may also be subjected to post-treatments to incorporate additional functionalities that improve the adsorption capacity (Qasem et al., 2021).

Apart from the traditionally used thermal conversion processes, steam explosion (STEX) has attracted some attention during the last couple of years as a process of interest for adsorbent production. Whereas steam activation is a process for developing carbon materials porosity and functionalities, conducted at temperatures above 700 °C in an environment partially containing steam at low or moderate pressure, steam explosion is performed at lower temperatures (160–260 °C) at the corresponding steam saturation pressure. The process is terminated by rapidly reducing the pressure, leading to the explosive decompression of the lignocellulosic material. Together with the thermal treatment, which facilitates the degradation of hemicellulose and softening of lignin, the pressure release causes a structural breakdown of the biomass (Hoang et al., 2023). A study of coconut husks showed that STEX could be utilized in a single stage to produce an adsorbent superior to the raw coconut husk powder for the adsorption of $Cu^{2+}$ and $Cd^{2+}$, which was attributed to an increased crystallinity and porosity due to the thermal degradation of hemicellulose (Pinheiro Nascimento & Barros Neto, 2021). In another study, the authors used a similar process denoted hydrothermal-pressure preconditioning eruption in a multistage treatment. Pine sawdust was preconditioned and then steam-activated by pyrolysis at 900 °C. The resulting carbons could be used for perfluorooctanoic acid and methylene blue adsorption, where they outperformed a commercial activated carbon in adsorption capacity (Yang & Cannon, 2021). In contrast, the adsorption of $Ni^{2+}$ from simulated wastewater onto steam-exploded poplar was used in another study utilizing multistage treatments. By pyrolysis of the biomass-nickel residue, a Ni-doped carbon fiber with a surface area of 1480 m$^2$/g could be produced (Yang et al., 2021). However, the few studies present in the literature using STEX as a pretreatment have all employed lab-scale batch process conditions while the industrial standard uses continuous operations.

Adsorption is widely used for water purification as it is versatile, cost-efficient, and relatively easy to set up and operate (Bilal et al., 2022; Praveen et al., 2022; Qasem et al., 2021). At the same time, an ever-growing textile industry (Textile Exchange, 2022) and increased environmental awareness have put focus on the vast amounts of dyehouse effluents generated by this industry (Kant, 2012). The dye-containing wastewater threatens aquatic environments and, ultimately, human health. Azo dyes, for example, are commonly employed for dyeing textiles and are suspected to be carcinogenic due to the formation of aromatic amines during their degradation (Al-Tohamy et al., 2022). Reactive orange 16 (RO16) is a frequently used azo dye, and several authors have investigated its adsorption onto a variety of adsorbents (Calvete et al., 2010; dos Reis et al., 2021b; dos Santos et al., 2014; Malakootian & Heidari, 2018; Marrakchi et al., 2017; Rosa et al., 2008; Shah et al., 2020; Won et al., 2006). For example, dos Reis et al., 2021b, worked with biobased activated carbons from softwood bark (*Picea abies*) produced via activation with KOH and $ZnCl_2$ and could reach a Langmuir maximum adsorption capacity of 355 and 90 mg g$^{-1}$

respectively. Softwood bark is considered an underused resource mainly utilized for low-value applications (dos Reis et al., 2021b) and was thus selected as raw material for this work.

This investigation aimed to study the effect of novel semi-industrial STEX preconditioning of softwood bark for producing functionalized ACs for adsorption. The impact of STEX treatment before $ZnCl_2$-activation at two carbonization temperatures on produced AC characteristics such as morphology, specific surface area and porosity, surface chemistry, AC composition, and adsorption of RO16 and two synthetic dyehouse effluents were evaluated.

## 2. Materials and methods

### 2.1. Raw material and preprocessing

The raw material used in the study was a mixed industrial bark of Norway spruce (*Picea abies*) and Scots pine (*Pinus Sylvestris*) from a pulp mill in northern Sweden. The bark was shredded, and the screened fraction <14 mm was selected for the steam treatments. A junk trap removed sand and gravel from the bark before the steam explosion (STEX) treatments. Additional details regarding the sampling and preparations are reported elsewhere (Averheim et al., 2022).

#### 2.1.1. Steam explosion

A pilot system for continuous STEX (Valmet BioTrac, Valmet AB, Sundsvall, Sweden) was used to precondition the already shredded bark. The system is described in detail in the literature (Averheim et al., 2022), and the schematic illustration is available in the e-supplementary material. The bark was processed at 200 °C reactor temperature at a residence time of 10 min. The feed rate was approximately 52 kg h$^{-1}$ on a dry basis (127 kg h$^{-1}$ on an as-received basis at 41 % total solids content).

Sulphuric acid, 37 % (Swed Handling AB, Sweden), diluted to 8.1 % (w/v), was added to the biomass in the atmospheric part of the pretreatment system to reach 3.8 % (w/w) sulphuric acid dose on raw material total solids. The sulphuric acid going into the reactor was 2.2 % (w/w), accounting for the acidity of the liquid pressed out from the plug screw.

Sampling was conducted from the discharge cyclone during steady-state operation (>60 min of operation at a stable temperature and feed rate). Steam-exploded material was then collected for 5 min for further evaluation. Ten reference samples of the unprocessed bark were also collected from the outlet of the raw material buffer bin and were mixed into a composite sample. The steam-exploded and reference barks were dried at 45 °C to constant weight and stored in sealed plastic bags at 4 °C before further treatment or characterization.

#### 2.1.2. Characterization of raw and steam-exploded bark

The carbohydrate composition of the raw reference bark and steam-exploded bark was determined following National Renewable Energy Laboratory (NREL) laboratory analytical procedures (Hames et al., 2008; Sluiter et al., 2008) and ash content according to ISO 18122:2015. A spectrophotometer (Agilent Cary UV-100) was used for the determination of acid-soluble lignin at 205 nm using 110 L g$^{-1}$ cm$^{-1}$ as extinction coefficient, and the neutral carbohydrates were quantified through ion chromatography (Dionex ICS-3000 with CarboPac PA-1 precolumn and analysis column).

### 2.2. Preparation of carbon materials

The reference bark was ground in a Retsch SM 200 knife mill (Retsch GmbH) with a 5 mm screen sieve, followed by a Fritsch Pulversisette 14 mill (Fritsch GmbH) equipped with a 0.5 mm sieve. The SE material was ground directly in the Fritsch Pulverisette using the 0.5 mm sieve. By visual inspection, this material already had a small particle size but was still ground for fair comparison with the reference material.

Activation and pyrolysis were then conducted according to principles described in the literature (dos Reis et al., 2021a). The reference bark and the steam-exploded bark were mixed with the activation chemical $ZnCl_2$ at a mass ratio 1:1 on a dry basis (20 g biomass per test). Milli-Q water was added under continuous stirring until a thick, homogenous paste was formed. The paste was allowed to soak for two hours, whereafter, the paste was left in an oven to dry at 60 °C overnight. Samples were then pyrolyzed at 600 or 800 °C in a reactor heated by a furnace. Nitrogen gas was used to keep an inert atmosphere during the process. The heating rate was 10 °C min$^{-1}$ and the desired temperature was kept for one hour. The oven was then cooled to <100 °C before the nitrogen purge was turned off, and the samples were removed and left to cool to ambient temperature.

The pyrolyzed samples were weighed and ground using a Fritsch Pulversisette 14 mill (Fritsch GmbH) equipped with a 0.2 mm sieve. Acid washing was conducted to remove residues of the activation chemical. The materials were put in a flask connected to a re-condenser with 6 M HCl and kept at 70 °C under agitation for two hours. The slurry was dewatered over a glass microfiber filter (Whatman GF/A grade), and the solid was resuspended in hot Milli-Q water and washed repeatedly to a constant pH of the filtrate. The washed carbons were dried at 105 °C and then weighed and stored in sealed plastic tubes.

Four carbon materials were produced, two from raw bark (AC 600 and AC 800) and two from steam-exploded bark (AC-SE 600 and AC-SE 800), where 600 and 800 denote the pyrolysis temperature.

### 2.3. Characterization of carbon materials

$N_2$ isotherms were measured with a sorptometer (Tristar, Micrometrics Instrument Corporation) to obtain the specific surface area ($S_{BET}$), pore volume, meso- ($S_{MESO}$), and micropore area ($S_{MICRO}$) for the carbon materials.

XPS was conducted for C1s (280–298 eV), O1s (525–545 eV), and S2p (157–175 ev) using a Thermo Scientific ESCALAB 250Xi XPS system equipped with an Al Kα X-ray source. The measurements were performed using standard protocols (dos Reis et al., 2021a). No S2p signals were detected in samples AC 600 and 800 during the XPS spectral survey, and consequently, these samples were not scanned in detail for S2p.

Raman spectra were recorded using a Bruker BRAVO handheld unit with its vial accessory to determine the degree of graphitization ($I_D/I_G$). A full spectral range recording (300–3200 cm$^{-1}$) at a resolution of 2 cm$^{-1}$ was conducted, with integration time set on automatic mode. Single scans were recorded for every sample and collected in the OPUS version 5 software (Bruker Corporation). Data processing was conducted in MATLAB R2021b (MathWorks) with the open-source graphical user interface available from the Vibrational Spectroscopy Core Facility at Umeå University (https://www.umu.se/en/research/infrastructure/visp/downloads/). The spectral range was trimmed to 1000–1900 cm$^{-1}$, and a total area normalization with Savitzy-Golay filtering polynomial order = 1 and frame rate = 7 was performed. No baseline correction was needed. Peak fitting was finally conducted in Origin Pro 2020b to separate the D and G peaks from other peaks relating to disorder (Sadezky et al., 2005), and $I_D/I_G$ was calculated from their integrated areas.

Fourier transform infrared (FTIR) spectra were recorded in attenuated total reflection (ATR) mode using a Thermo Scientific Nicolet iS5 FTIR spectrometer equipped with a Ge crystal designed for measuring highly colored samples. Spectra were recorded in 600–4000 cm$^{-1}$ wavelength range with a 0.5 cm$^{-1}$ step size. The surface morphology was analyzed using scanning electron microscopy (SEM) (Carl Zeiss Evo SEM) with an acceleration voltage of 5 kV and magnification ranging from 5 k to 25 k.

### 2.4. Dye adsorption testing and regeneration

Adsorption testing was performed on synthetic effluents with reactive orange 16 dye (RO16) and mixed effluents A and B (see section 2.4.1). A batch adsorption procedure was used, where the carbon materials were contacted with the effluent at an adsorbent dosage of 1.5 g/L under continuous mixing (IKA KS250 laboratory shaker) at ambient temperature for a predetermined time ($t$). After that, the adsorption process was stopped by centrifugation in a Sorvall ST16R centrifuge and decanting the supernatant. For tests with RO16, the initial concentration of the effluent ($C_i$) and the final concentration of the supernatant ($C_f$) was determined with a Shimadzu UV-1800 UV/visible scanning spectrophotometer by measuring absorbance at 494 nm. For the mixed effluents (A and B), a spectral scan in the range 180–800 nm was performed to determine the total chromophore removal.

Testing was conducted to determine RO16 adsorption kinetics ($C_i$ = 200 mg/L, and $t$ = 0.1 to 4 h), and equilibrium ($C_i$ = 30–1000 mg/L, and $t$ = 19 h). Total chromophore removal from effluents A and B was performed at $t$ = 19 h. All testing was conducted at pH 6. The formulation and calculation of adsorption isotherms and kinetics are described in the e-supplementary material.

For the regeneration tests, the active carbons that showed the best performance were loaded using RO16 solution (400 mg/L). Loaded carbons underwent water rinse to eliminate any residual unadsorbed dye. Subsequently, they were dried overnight at 50 °C in an oven. The dried loaded carbons were exposed to a solution containing 0.2 M NaOH and 20 % EtOH, followed by agitation for 12 h to facilitate the desorption of the dye. The separated dye was then isolated from the carbon, which underwent multiple rinses with water to eliminate any remaining eluent. Afterwards, it was dried overnight at 50 °C. The dye removal capacity of the regenerated adsorbent was then reassessed. This process was repeated for four consecutive cycles of adsorption and desorption.

#### 2.4.1. Preparation of mixed effluents

The mixed effluents A and B each consisted of eight dyes, mainly of Azo type, in the presence of sodium dodecyl, sodium acetate, sodium sulfate, and ammonium chloride. The pH of the effluents ranged between 5.2 and 5.4. The specified composition of the effluents is found elsewhere (dos Reis et al., 2023a).

## 3. Results and discussion

### 3.1. Composition of preprocessed materials

The composition of the raw material before activation and pyrolysis, Table 1, may impact the yield and properties of the AC and was thus analyzed. The raw bark consisted mainly of cellulose, hemicellulose, and lignin, but also a significant fraction of uncharacterized substances (14.8 %). Based on the literature, this uncharacterized fraction chiefly constitutes a variety of extractives, such as tannin and acidic sugars found in pectin (Le Normand et al., 2014). STEX is known to hydrolyze and degrade the hemicelluloses, a mechanism especially pronounced with an acid catalyst present (Hoang et al., 2023), which was confirmed in this work. The STEX treatment altered the composition significantly, with a decrease in neutral sugars due to the degradation of hemicelluloses, Table 1. Concomitantly, the lignin content increased drastically due to the removal of other components, but potentially also due to

**Table 1**
Composition of the raw and steam-exploded bark as a percentage of its dry weight. Neutral carbohydrates summarise the cellulose and hemicellulose content and are reported based on the anhydro-monomeric mass, while total lignin summarises the acid-soluble and acid-insoluble lignin.

| Compounds | Raw bark | Steam-exploded bark |
|---|---|---|
| Neutral carbohydrates | 50.5 | 44.5 |
| Total lignin | 32.0 | 49.9 |
| Ash content | 2.7 | 2.5 |
| Other | 14.8 | 3.1 |

pseudo-lignin formation. Pseudo-lignin is an acid-insoluble degradation product formed from the degradation of hemicellulosic sugars into diols and furans (Aarum et al., 2019). In addition, the phenolic tannins found in the bark can also condense to form acid-insoluble residues, contributing to the Klason lignin (Torget et al., 1991). Altogether, this may explain the elevated lignin content in the steam-exploded bark and the lowering of the non-qualitative fraction named "other" in Table 1.

### 3.2. Properties and yield of activated carbon materials

The degree of graphitization ($I_D/I_G$) determined from Raman spectra is widely employed for evaluating the microstructure of carbon materials (Merlen et al., 2017). $I_D/I_G$ is the ratio between the G band, found around 1582 cm$^{-1}$ indicating sp$^2$ hybridized carbon (graphitic structure), and the D band, around 1350 cm$^{-1}$ related to a more defective sp$^3$ hybridized carbon structure (Pimenta et al., 2007; Sadezky et al., 2005).

The spectra from the ACs prepared from bark are shown in Fig. 1. Apart from the D and G peaks, the spectra clearly revealed a third peak around 1186–1196 cm$^{-1}$ (Sadezky et al., 2005) which was separated from the D band through peak fitting before calculating $I_D/I_G$ (Table 2). Steam-exploded bark carbons (AC-SE 600 and 800) expressed an apparent intensification of the G peak in relation to the D peak compared to those prepared from raw bark (AC 600 and 800) and the lowest $I_D/I_G$ (1.08) was achieved at 600 °C with the steam-exploded bark. The steam-exploded precursor had a higher degree of aromaticity due to the elevated lignin content (Deng et al., 2016) compared to the raw bark, which may explain the more pronounced graphitization for these materials. Furthermore, carbons produced at 800 °C had a higher $I_D/I_G$ than carbons pyrolyzed at 600 °C, indicating a more disordered structure. Moreover, FTIR spectra from the ACs (Fig. 1e) provided limited information regarding the influence of steam-explosion on AC properties.

One of the essential characteristics of any carbonaceous material is its porosity, e.g., the $S_{BET}$, $S_{MESO}$, and $S_{MICRO}$, as well as pore volume. These porous features, shown by SEM in the e-supplementary material, significantly influence the materials' ability to adsorb pollutants by adsorption. Table 2 shows the biobased materials' porosity data, i.e., $S_{BET}$, $S_{MESO}$, and $S_{MICRO}$, pore volume, and pyrolysis mass yield. The results show that the samples subjected to STEX exhibited higher $S_{BET}$ values. A possible explanation is that when a sample is subjected to STEX, its structure opens up (Muzamal et al., 2015), increasing the contact area available for the chemical activator, which, in turn, provokes an increase in the $S_{BET}$ value.

Table 2 also shows that STEX treatment did shift the micro-mesoporosity interrelational pore structure slightly towards a more microporous structure. In addition, it was responsible for an 11 % and 21 % pore volume increase for the samples pyrolyzed at 600 and 800, respectively. These results suggest that STEX influenced the textural properties of bio-based carbons. Adsorbents with higher $S_{BET}$ and pore volume are promising candidates for adsorption applications (Dąbrowski, 2001).

X-ray photoelectron spectroscopy (XPS) was used to investigate the surface composition and functionality of the carbons further. The XPS survey spectra revealed the self-evident presence of carbon (C) and oxygen (O) in all carbons, whereas the STEX-pretreated carbons also contained weak signals of sulfur (S) (Fig. 1). Spectral deconvolution of S2p correlated to thiophene (C − S − C, 164.1–164.2 eV), sulfoxide (C − SO − C, 165.3–165.4 eV), sulfone (167.7–167.9 eV), and sulfate (169.1–169.3 eV). These sulfur states imply an abundance of functional groups that have the potential to enhance the adsorptive capacity of the STEX-pretreated carbons (Vigneshwaran et al., 2021). Analysis of the FTIR data (Fig. 1e) concerning sulfur functionalities was inconclusive, which may be explained by a low sulfur concentration. Apart from sulfur
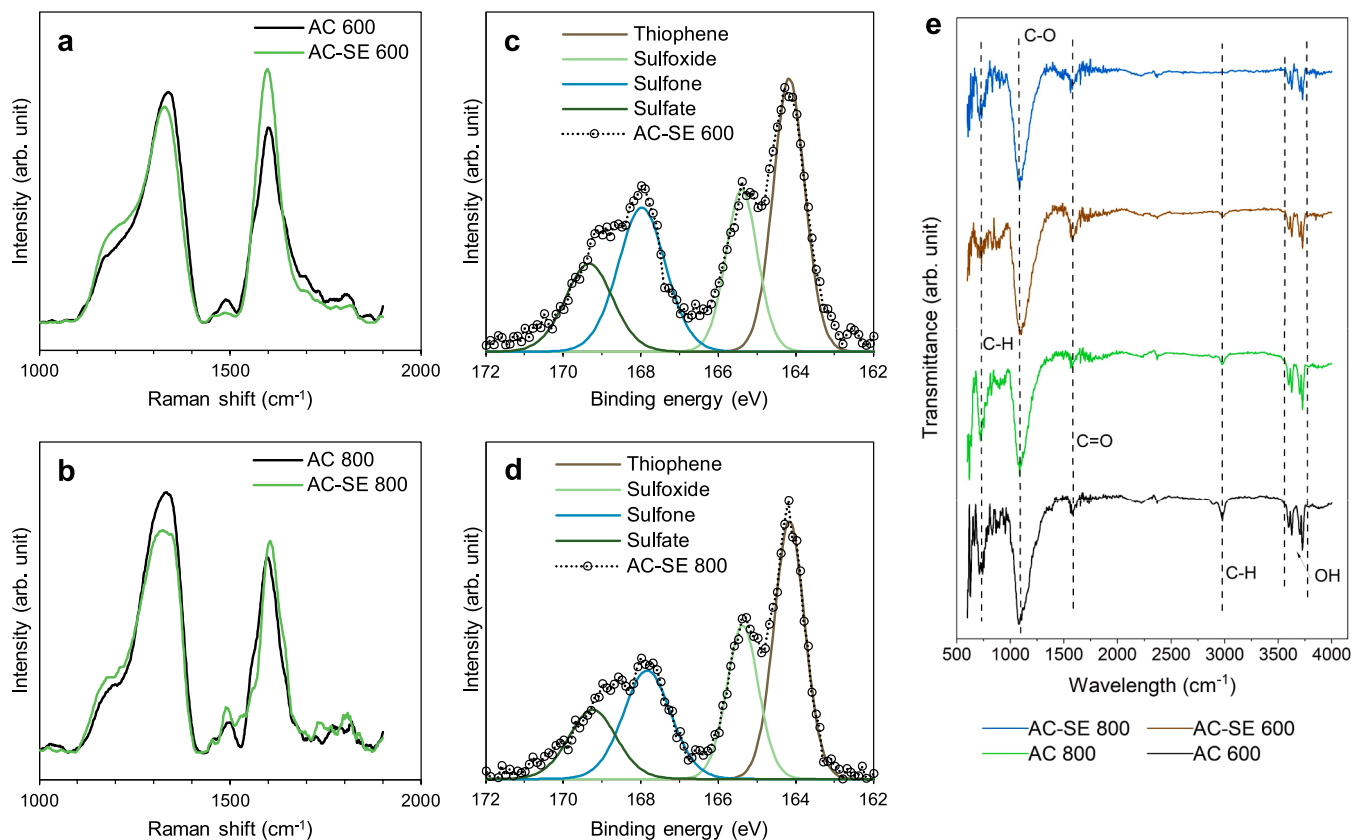


**Fig. 1.** Raman spectra from AC:s pyrolyzed at 600 (a) and 800 °C (b) and S2p XPS spectra for steam-exploded AC:s pyrolyzed at 600 (c) and 800 °C (d) and FTIR spectra of pyrolyzed AC:s (e).

**Table 2**

Textural properties and pyrolysis yield for the bark AC:s. The degree of graphatization $I_D/I_G$ is expressed as a ratio of the integrated areas of the D and G peaks.

| Sample | $S_{BET}$ | $S_{MESO}$ | $S_{MICRO}$ | $S_{MESO\%}$ | $S_{MICRO\%}$ | Pore volume | $I_D/I_G$ | Mass yield |
|---|---|---|---|---|---|---|---|---|
| | $(m^2\,g^{-1})$ | $(m^2\,g^{-1})$ | $(m^2\,g^{-1})$ | (%) | (%) | $(cm^3\,g^{-1})$ | (–) | (%) |
| AC 600 | 1217 | 615 | 602 | 50.5 | 49.5 | 0.27 | 1.41 | 40 |
| AC 800 | 1018 | 490 | 528 | 48.2 | 51.8 | 0.24 | 2.03 | 36 |
| AC-SE 600 | 1308 | 645 | 662 | 49.3 | 50.7 | 0.30 | 1.08 | 36 |
| AC-SE 800 | 1217 | 535 | 682 | 44.0 | 56.0 | 0.29 | 1.81 | 29 |

functionalities, the XPS peak table (found in the e-supplementary material) revealed a higher fraction of C-C bonds for AC-SE 600 than the other carbon materials. The elevation of C-C bonds is likely caused by graphitic structures being especially pronounced in AC-SE 600, indicated by its degree of graphitization (Table 2).

High lignin content positively impacts biochar yields from pyrolysis without activation chemicals (Cagnon et al., 2009). However, the mass yield (Table 2) was somewhat lower for AC-SE than the AC at the corresponding temperature, although it had a higher lignin content. The lower yield may indicate a more efficient impregnation, promoting reactivity and pore formation. Consequently, yield decreases, but quality parameters improve due to a more homogenous treatment and efficient use of the activation agent.

*3.3. Adsorption kinetics*

Fig. 2 shows the profiles of the RO16 adsorption kinetics for the carbon materials. The curves display similar trends regardless of temperature and STEX treatment. However, the samples subjected to STEX adsorbed more RO16 molecules than the AC samples pyrolyzed at the corresponding temperature. The better adsorption performances of the SE–AC samples could be related to their higher specific surface areas and larger pore volumes. For instance, high $S_{BET}$ means more accessible, active sites for the adsorption of RO16 molecules, promoting the adsorptive properties.

The kinetic behavior was further evaluated by assessing the models' suitability, considering $R^2_{adj}$ and *SD* values (dos Reis et al., 2023a). The kinetic model parameters and statistical information are presented in Table 3. General order best described the RO16 uptake, based on $R^2_{adj}$ and *SD*, within the studied timeframe (0–360 min). The general order equation determines the apparent reaction order based on the experimental data (dos Santos et al., 2014), making it a versatile function that can be fitted to many different cases (Guo & Wang, 2019). However, the maximum uptake (Table 3) estimated by this model reaches higher than the theoretical maximum (200 mg g$^{-1}$) for the carbons pyrolyzed at 800 °C and values much higher than those obtained after 19 h for the 600 °C carbons. This overprediction may be due to the complexity of the adsorption onto microporous materials where the adsorption rate is governed by four major phenomena, specifically external and internal mass transfer, surface diffusion, and the adsorption/desorption elementary process (Dąbrowski, 2001). An intraparticle diffusion (IPD) model (Weber & Morris, 1963) was applied to describe the adsorption process by investigating the linear regions of $q_t$ as a function $t^{0.5}$. The modeling is further described in the e-supplementary material, and the
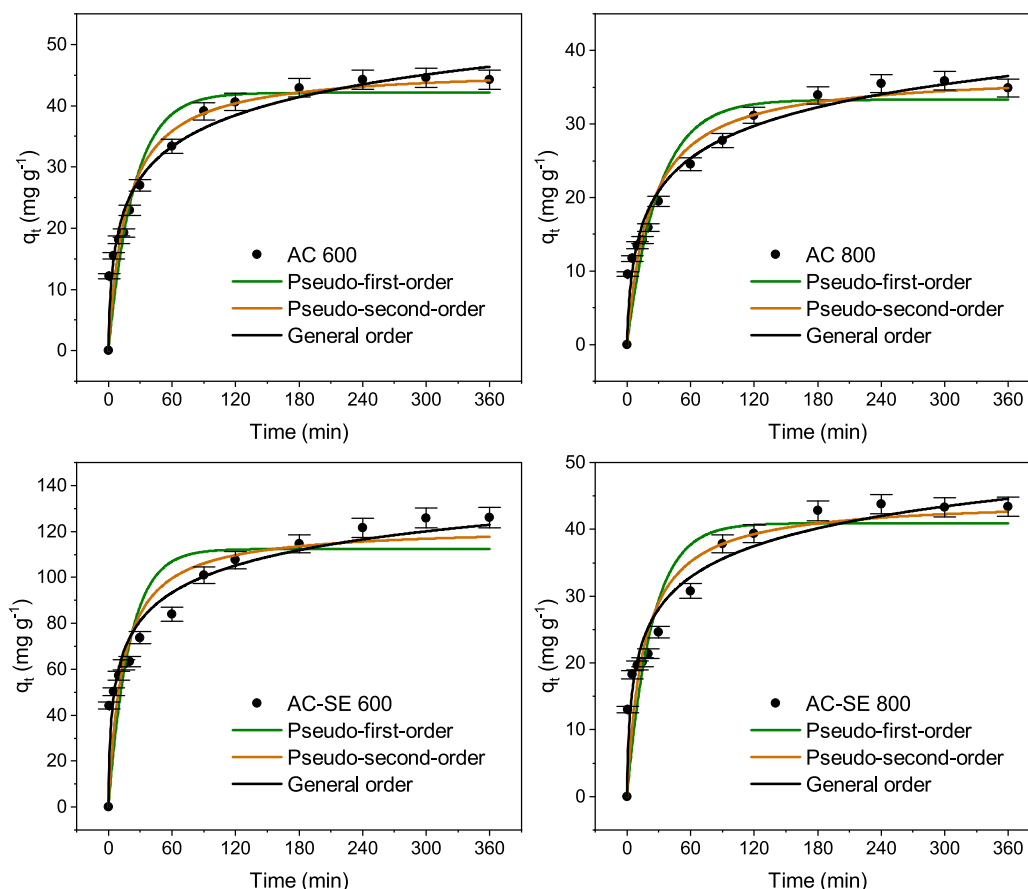


**Fig. 2.** Kinetic models and experimental data for RO16 adsorption.

**Table 3**
Kinetic model parameters for RO16 adsorption.

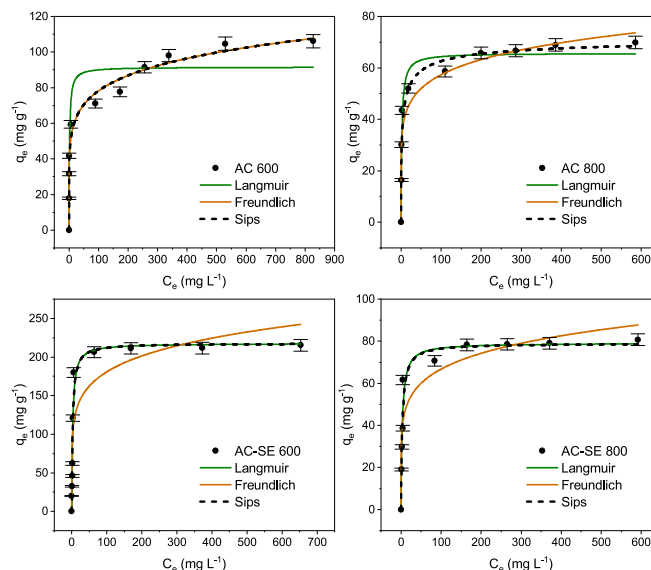|  | AC 600 | AC 800 | AC-SE 600 | AC-SE 800 |
|---|---|---|---|---|
| **Pseudo-first-order** | | | | |
| $q_1$ (mg g$^{-1}$) | 42.1 | 33.3 | 112 | 40.9 |
| $k_1$ (min$^{-1}$) | $4.14 \times 10^{-2}$ | $3.33 \times 10^{-2}$ | $5.04 \times 10^{-2}$ | $4.24 \times 10^{-2}$ |
| $R^2$ | 0.912 | 0.892 | 0.798 | 0.848 |
| $R^2_{adj}$ | 0.904 | 0.883 | 0.781 | 0.835 |
| $SD$ (mg g$^{-1}$) | 4.47 | 3.94 | 17.4 | 5.59 |
| **Pseudo-second-order** | | | | |
| $q_2$ (mg g$^{-1}$) | 46.2 | 37.1 | 122 | 44.5 |
| $k_2$ (g mg$^{-1}$ min$^{-1}$) | $1.24 \times 10^{-3}$ | $1.21 \times 10^{-3}$ | $6.01 \times 10^{-3}$ | $1.40 \times 10^{-3}$ |
| $R^2$ | 0.947 | 0.934 | 0.875 | 0.904 |
| $R^2_{adj}$ | 0.943 | 0.929 | 0.864 | 0.896 |
| $SD$ (mg g$^{-1}$) | 3.46 | 3.08 | 13.7 | 4.43 |
| **General order** | | | | |
| $q_n$ (mg g$^{-1}$) | 236 | 169 | 352 | 177 |
| $k_n$ (g mg$^{-1}$)$^{n-1}$ (min$^{-1}$) | $1.84 \times 10^{-65}$ | $7.89 \times 10^{-51}$ | $3.66 \times 10^{-39}$ | $6.65 \times 10^{-49}$ |
| $n$ (−) | 27.7 | 22.8 | 15.7 | 21.9 |
| $R^2$ | 0.969 | 0.963 | 0.950 | 0.955 |
| $R^2_{adj}$ | 0.964 | 0.956 | 0.941 | 0.947 |
| $SD$ (mg g$^{-1}$) | 2.75 | 2.42 | 9.05 | 3.17 |
| **IPD (0–120 min)** | | | | |
| $C$ (mg g$^{-1}$ min$^{-0.5}$) | 8.90 | 6.58 | 36.3 | 10.6 |
| $k_p$ (mg g$^{-1}$) | 3.05 | 2.24 | 6.53 | 2.68 |
| $R^2$ | 0.989 | 0.994 | 0.993 | 0.985 |
| $R_i$ | 0.78 | 0.79 | 0.66 | 0.73 |

model constants are shown in Table 3. The investigation revealed two initial zones, the first one <1 min related to boundary layer diffusion to the external surface of the adsorbents, quantified by the constant $C$, and the second one 1–120 min related to intraparticle diffusion described by the IPD rate constant $k_p$ (Bhat et al., 2023). The constant, $C$, was positive for all tested carbon materials. Thus, reaction kinetics for RO16 removal were governed by the combined boundary layer and intraparticle diffusion effect.

In literature, the adsorption of RO16 onto a variety of biobased carbon materials is modeled as general order (dos Reis et al., 2021b; dos Reis et al., 2023a; dos Santos et al., 2014) as well as pseudo-second-order (Malakootian & Heidari, 2018; Marrakchi et al., 2017; Rosa et al., 2008; Shah et al., 2020). In this study, the pseudo-second-order was the second-best model, followed by the pseudo-first-order, which was poorly adapted to the experimental data, judging from $R^2_{adj}$ and $SD$. The fact that pseudo-second-order could be reasonably adapted to the data implies that chemisorption was rate-limiting. However, different potential adsorbent-adsorbate chemical interactions and pore diffusion add to the complexity (Lin et al., 2023; Sutthasupa et al., 2023).

### 3.4. Adsorption equilibria

Adsorption isotherms are helpful tools for describing and understanding how adsorbates interact with adsorbents. Numerous adsorption isotherm models have been proposed over the years (Al-Ghouti & Da'ana, 2020; Foo & Hameed, 2010). Langmuir, Freundlich and Sips models were employed in this work to study the equilibria.

The isotherms and their parameters are displayed in Fig. 3 and Table 4. The figure shows that the samples subjected to STEX (AC-SE 600 and AC-SE 800) reached a plateau at a lower initial effluent concentration than those without STEX, especially pronounced at 600 °C pyrolysis temperature. Meanwhile, the % Removal was higher for the STEX-treated carbons compared to the reference at the corresponding temperature, which could be explained by the higher BET surface area and, potentially, additional functionalities.



**Fig. 3.** Isotherm models based and experimental data for RO16 adsorption.

**Table 4**
Equilibrium isotherm model parameters for RO16 adsorption.

|  | AC 600 | AC 800 | AC-SE 600 | AC-SE 800 |
|---|---|---|---|---|
| **Freundlich** | | | | |
| $k_F$ (mg g$^{-1}$)(L mg$^{-1}$)$^{1/nF}$ | 39.0 | 29.8 | 88.1 | 32.9 |
| $n_F$ (−) | 6.61 | 7.05 | 6.41 | 6.51 |
| $R^2$ | 0.958 | 0.924 | 0.844 | 0.897 |
| $R^2_{adj}$ | 0.953 | 0.915 | 0.827 | 0.884 |
| $SD$ (mg g$^{-1}$) | 7.92 | 7.11 | 36.7 | 10.0 |
| **Langmuir** | | | | |
| $Q_{max}$ (mg g$^{-1}$) | 91.6 | 65.7 | 218 | 79.2 |
| $K_L$ (L mg$^{-1}$) | 0.573 | 0.467 | 0.372 | 0.312 |
| $R^2$ | 0.892 | 0.935 | 0.949 | 0.960 |
| $R^2_{adj}$ | 0.879 | 0.927 | 0.943 | 0.955 |
| $SD$ (mg g$^{-1}$) | 12.7 | 6.57 | 21.0 | 6.26 |
| **Sips** | | | | |
| $Q_{ms}$ (mg g$^{-1}$) | $6.43 \times 10^3$ | 72.8 | 218 | 79.0 |
| $K_S$ (L mg$^{-1}$) | $6.09 \times 10^{-3}$ | 0.516 | 0.372 | 0.304 |
| $n_S$ (−) | 0.153 | 0.537 | 1.00 | 1.00 |
| $R^2$ | 0.958 | 0.943 | 0.949 | 0.960 |
| $R^2_{adj}$ | 0.947 | 0.927 | 0.936 | 0.948 |
| $SD$ (mg g$^{-1}$) | 8.40 | 6.58 | 22.3 | 6.71 |

Analogous to the kinetic evaluation, the suitability of the models was determined based on $R^2_{adj}$ and $SD$. Generally, Sips was the model that best could explain the experimental data for the four different carbons. The Sips isotherm model combines the Langmuir and Freundlich isotherm model (Al-Ghouti & Da'ana, 2020; Foo & Hameed, 2010), which explains its adaptability in this case. However, studying the individual carbons, Langmuir was an equally good fit for the experimental data for the SE-AC samples, indicating homogenous adsorption (Foo & Hameed, 2010). On the contrary, the RO16 uptake on AC samples did not plateau in the same way with increasing concentration (Fig. 3), and AC 600 could be well fitted with the Freundlich isotherm. Adaptation to the Freundlich isotherm could indicate a more heterogeneous surface and multilayer adsorption (Foo & Hameed, 2010). The difference in adsorption equilibria between SE-AC and AC suggests that SE-AC have equally energized adsorption sites (Bhat et al., 2023), whereas this is less pronounced for the AC samples. Although the uptake increased with increasing concentration for AC 600 long after AC-SE 600 was saturated with adsorbate, its % Removal was always inferior to AC-SE 600 due to

the high amount of residual dye left in solution at higher adsorbate concentrations. AC-SE 600 was thus the best AC for RO16 removal in this study, with a Langmuir maximum uptake of 218 mg g$^{-1}$.

The performance, in terms of Langmuir maximum RO16 uptake ($Q_{max}$), of the carbons AC 600, AC 800, and AC-SE 800 is similar to other carbons made from softwood bark with ZnCl$_2$ as an activator (dos Reis et al., 2021b), while AC-SE 600 on the other hand stands out as a more than twice as promising adsorbent. A compilation of $Q_{max}$ for some other biobased adsorbents in literature is presented in the e-supplementary material. A few of the carbons display $Q_{max}$ values higher than AC-SE, such as AC from spruce bark activated with KOH (dos Reis et al., 2021b), Se-doped biochar from spruce bark (dos Reis et al., 2023a),

carbonized Brazilian-pine fruit shell (Calvete et al., 2010) and cross-linked quaternary chitosan salt (Rosa et al., 2008). The latter stands out with an uptake as high as 1060 mg g$^{-1}$.

However, the magnitude of the textile industry and its potential need for wastewater treatment (Al-Tohamy et al., 2022) calls for cheap bulk adsorbents with a good enough performance. One of the exciting features of AC-SE 600 is the high mass yield (36 %) compared with, for example, KOH-activated spruce bark (14 %) (dos Reis et al., 2021b). Furthermore, its processing is based on a novel STEX technology, an abundant raw material, and relatively cheap chemicals (H$_2$SO$_4$ and ZnCl$_2$), which makes steam-exploded activated carbons an interesting prospect for the future.
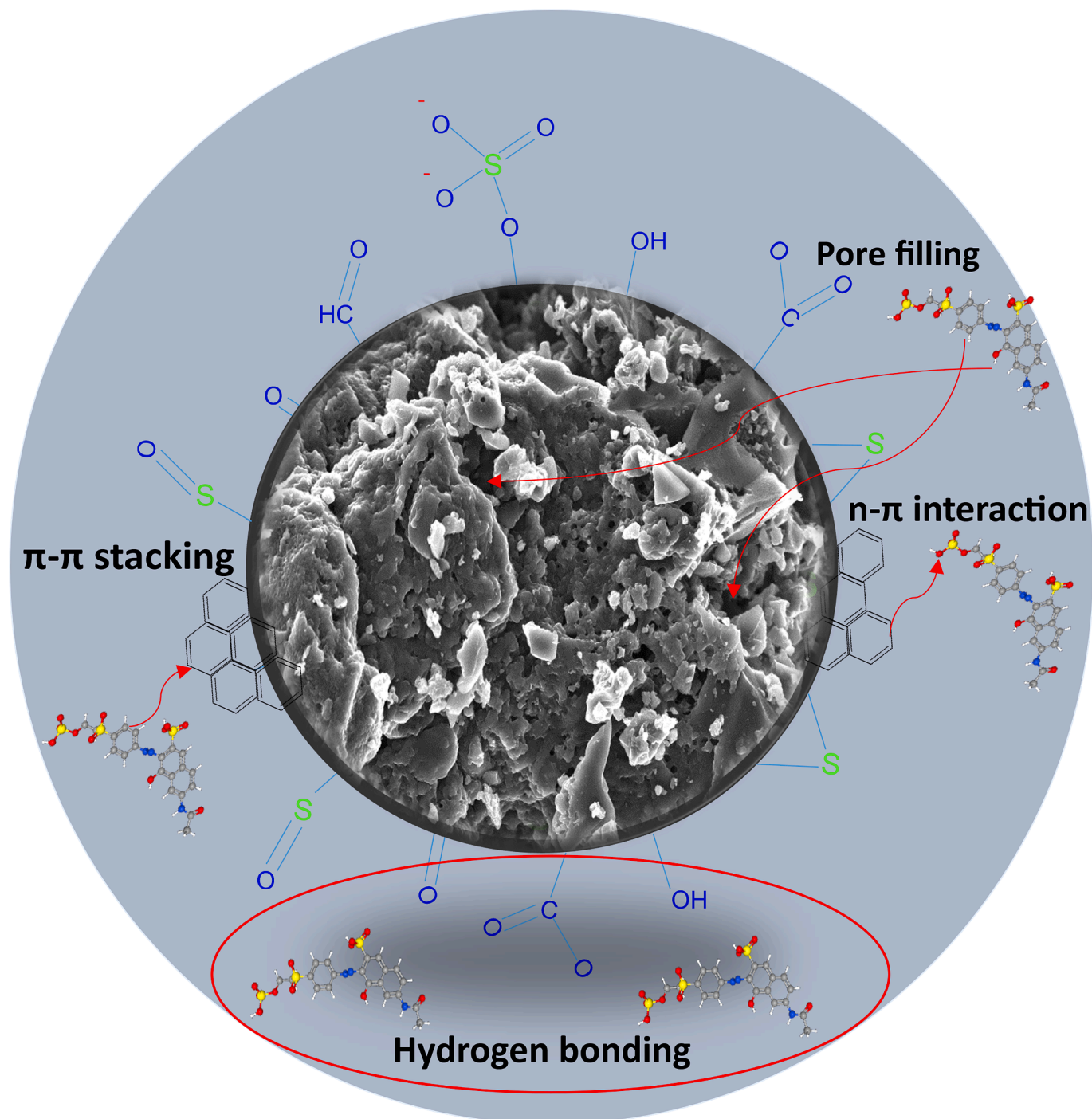


**Fig. 4.** Possible mechanisms for adsorption of RO16 onto carbon adsorbent.

## 3.5. Adsorbent regeneration

The AC-SE 600 °C and the AC 600 °C were used to evaluate the regeneration studies. The tests were performed using an adsorbent dosage of 2.5 g/L available in the e-supplementary material. The AC-SE 600 carbon performed better compared to the AC 600, and results showed that it can be reused at least three times, losing approximately 40 % of its initial removal performance. This loss of performance could be due to pore blockage by adsorbate molecules getting sized inside small pores, as well as mechanical damage to the carbon matrix during cycling. To sum up, the AC-SE 600 biochar exhibited good reusability for a second cycle. However, further experiments on testing different eluents could help the biochar to reach even higher adsorption performances after two or more cycles.

## 3.6. Possible adsorption mechanisms of RO16 on carbon adsorbents

XPS performed on a dye-loaded sample (AC-SE 600) showed higher amounts of S, N, O, and Na (all constituents of RO16), validating the dye adsorption on the carbon surface (e-supplementary material). Spectral deconvolution revealed amide (O = C-NH, 531.8 eV) and sulfonate ($SO_3$, 167,4 eV) functionalities, only present in the dye-loaded sample. Fig. 4 shows a proposal of the interaction mechanism of RO16 with carbon-based materials. Because the carbon adsorbents displayed very high surface areas, the dominant mechanism should be the pore filling. Furthermore, due to the RO16 molecule dimensions (1.68 nm (length), 1.42 nm (width)) (Calvete et al., 2010), it would be expected that RO16 molecule can easily fit into the big micropores (1.7 – 2.0 nm) and mesopores (>2.0 nm) present in the carbon adsorbents. Besides pore filling, hydrogen bonding, π- π stacking, and n- π interactions are also involved in the overall adsorption process. Hydrogen bonding occurs between H of the RO16 molecules and the carbon materials' O, H, and S atoms (dos Reis et al., 2023b). For the *π-π* interactions, RO16 has functionalities that can create a strong electron-withdrawing effect on the aromatic ring from the carbon, which allows the aromatic ring to bind to the electron donor carbon adsorbent surfaces that establish *π-π* interactions (Lima et al., 2024). Donor-acceptor interactions (n–π interaction) between the oxygen and sulfur (electron-donating) on the adsorbent surface and the π-system in the aromatic rings of the dye molecules (electron acceptor) could also contribute to the adsorption mechanism (Sayed et al., 2024).

## 3.7. Treatment of two synthetic dyehouse effluents

A real dyehouse effluent may contain various dyes, salts, and trace metals (Yaseen & Scholz, 2019). Therefore, the carbon materials potential for chromophore removal was tested on two synthetic effluents prepared from several dyes and salts (dos Reis et al., 2023b). UV–Vis spectra for the effluents before and after treatment and the % Removal of chromophores for the individual carbons are presented in Fig. 5. Analogous to the RO16 adsorption, AC-SE 600 was the best carbon for chromophore removal, achieving 71 and 73 % chromophore removal for effluent A and B, respectively. In contrast, the second-best carbon, AC 600, removed 48 and 54 %. These results show that the carbons are suited for the removal of a range of different dyes in a salt-containing environment. In addition, it highlights the benefit of subjecting the materials to STEX prior to a chemical activation step. This could be investigated further by optimizing the process for maximum yield and performance at minimum energy and chemical expenditure, investigating other activation chemicals and adsorbates, and even looking towards other carbon applications such as supercapacitors and batteries. Likewise, the importance of handling wasted adsorbents and desorbed pollutants sustainably, should be further studied and developed.
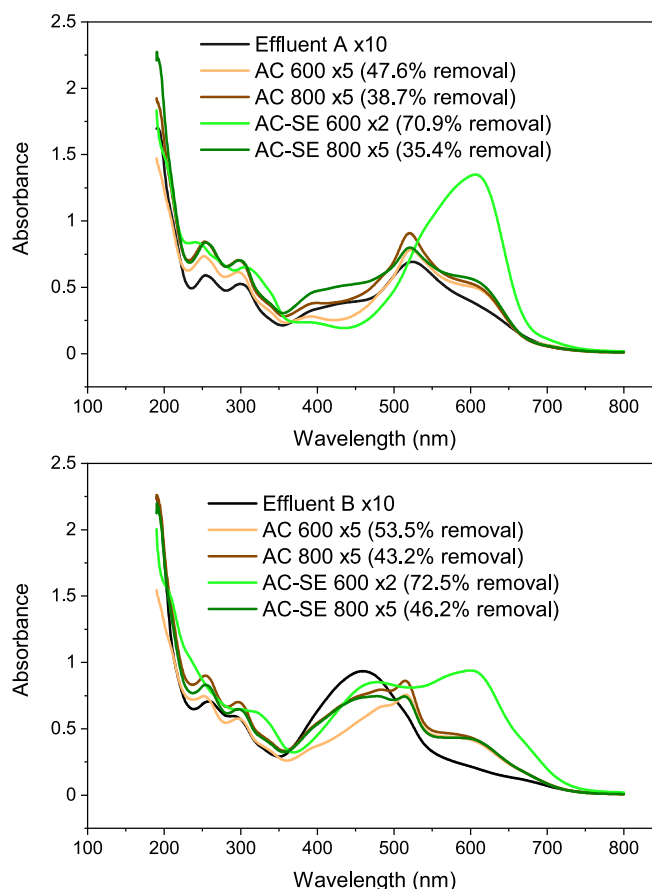


**Fig. 5.** UV–Vis spectra for the two synthetic dyehouse effluents A and B (ten times dilution) and residual effluent (two or five times dilution) after treatment with each of the four carbon materials. The % removal is calculated as a difference between the integrated curves before and after treatment.

## 4. Conclusions

This study demonstrated the feasibility of STEX preconditioning for softwood bark for producing functionalized ACs with high adsorption capacities. The STEX-treated carbons showed favourable characteristics with increased specific surface area, pore volume, and aromaticity, leading to enhanced adsorption compared to conventionally produced ACs. The adsorption kinetics and equilibrium studies revealed the effectiveness of the STEX-treated carbons in dye removal ($Q_{max}$ 218 mg g$^{-1}$). Moreover, the regeneration studies showed the potential for reusability of STEX-treated ACs. This research shows that innovative methods like STEX for producing carbonaceous adsorbents for wastewater treatment lay a foundation for future advancements in the field.

## CRediT authorship contribution statement

**Andreas Averheim:** Writing – original draft, Visualization, Investigation, Formal analysis, Conceptualization. **Glaydson Simões dos Reis:** Writing – review & editing, Validation, Methodology, Investigation, Conceptualization. **Alejandro Grimm:** Writing – review & editing, Investigation. **Davide Bergna:** Investigation. **Anne Heponiemi:**

Writing – review & editing. **Ulla Lassi:** Writing – review & editing, Resources. **Mikael Thyrel:** Writing – review & editing, Supervision, Resources, Project administration, Funding acquisition, Formal analysis, Conceptualization.

## Declaration of competing interest

The authors declare that they have no known competing financial interests or personal relationships that could have appeared to influence the work reported in this paper.

## Data availability

Data will be made available on request.

## Appendix A. Supplementary data

Supplementary data to this article can be found online at https://doi.org/10.1016/j.biortech.2024.130698.

## References

Aarum, I., Solli, A., Gunnarsson, H., Kalyani, D., Devle, H., Ekeberg, D., Stenstrøm, Y., 2019. Comparison of pyrolyzed lignin before and after milled wood lignin purification of Norway spruce with increasing steam explosion. Wood Sci. Technol. 53 (3), 601–618.

Al-Ghouti, M.A., Da'ana, D.A., 2020. Guidelines for the use and interpretation of adsorption isotherm models: A review. J. Hazard. Mater. 393, 122383.

Al-Tohamy, R., Ali, S.S., Li, F., Okasha, K.M., Mahmoud, Y.A.G., Elsamahy, T., Jiao, H., Fu, Y., Sun, J., 2022. A critical review on the treatment of dye-containing wastewater: Ecotoxicological and health concerns of textile dyes and possible remediation approaches for environmental safety. Ecotoxicol. Environ. Saf. 231, 113160.

Averheim, A., Larsson, S.H., Thyrel, M., 2022. Carbocation scavenger pretreatment to mitigate lignin self-condensation in a semi-industrial steam explosion process. Bioresource Technology Reports 20, 101292.

Bhat, S., Uthappa, U.T., Sadhasivam, T., Altalhi, T., Soo Han, S., Kurkuri, M.D., 2023. Abundant cilantro derived high surface area activated carbon (AC) for superior adsorption performances of cationic/anionic dyes and supercapacitor application. Chem. Eng. J. 459, 141577.

Bilal, M., Ihsanullah, I., Hassan Shah, M.U., Bhaskar Reddy, A.V., Aminabhavi, T.M., 2022. Recent advances in the removal of dyes from wastewater using low-cost adsorbents. J. Environ. Manage. 321, 115981.

Cagnon, B., Py, X., Guillot, A., Stoeckli, F., Chambat, G., 2009. Contributions of hemicellulose, cellulose and lignin to the mass and the porous properties of chars and steam activated carbons from various lignocellulosic precursors. Bioresour. Technol. 100 (1), 292–298.

Calvete, T., Lima, E.C., Cardoso, N.F., Vaghetti, J.C.P., Dias, S.L.P., Pavan, F.A., 2010. Application of carbon adsorbents prepared from Brazilian-pine fruit shell for the removal of reactive orange 16 from aqueous solution: Kinetic, equilibrium, and thermodynamic studies. J. Environ. Manage. 91 (8), 1695–1706.

Correa, C.R., Kruse, A., 2018. Biobased Functional Carbon Materials: Production, Characterisation, and Applications—A Review. Materials 11 (9), 1568.

Dąbrowski, A., 2001. Adsorption — from theory to practice. Adv. Colloid Interface Sci. 93 (1), 135–224.

Deng, J., Li, M., Wang, Y., 2016. Biomass-derived carbon: synthesis and applications in energy storage and conversion. Green Chem. 18 (18), 4824–4854.

dos Reis, G.S., Larsson, S.H., Mathieu, M., Thyrel, M., Pham, T.N., 2021a. Application of design of experiments (DoE) for optimized production of micro- and mesoporous Norway spruce bark activated carbons. Biomass Convers. Biorefin.

dos Reis, G.S., Larsson, S.H., Thyrel, M., Pham, T.N., Claudio Lima, E., de Oliveira, H.P., Dotto, G.L., 2021b. Preparation and application of efficient biobased carbon adsorbents prepared from spruce bark residues for efficient removal of reactive dyes and colors from synthetic effluents. Coatings 11 (7), 772.

dos Reis, G.S., Thivet, J., Laisné, E., Srivastava, V., Grimm, A., Lima, E.C., Bergna, D., Hu, T., Naushad, M., Lassi, U., 2023a. Synthesis of novel mesoporous selenium-doped biochar with high-performance sodium diclofenac and reactive orange 16 dye removals. Chem. Eng. Sci. 281, 119129.

dos Reis, G.S., Bergna, D., Grimm, A., Lima, E.C., Hu, T., Naushad, M., Lassi, U., 2023b. Preparation of highly porous nitrogen-doped biochar derived from birch tree wastes with superior dye removal performance. Physicochemical and Engineering Aspects, Colloids and Surfaces A, p. 669.

dos Santos, D.C., Adebayo, M.A., de Fátima Pinheiro Pereira, S., Prola, L.D.T., Cataluña, R., Lima, E.C., Saucier, C., Gally, C.R., Machado, F.M., 2014. New carbon composite adsorbents for the removal of textile dyes from aqueous solutions: Kinetic, equilibrium, and thermodynamic studies. Korean J. Chem. Eng. 31 (8), 1470–1479.

Foo, K.Y., Hameed, B.H., 2010. Insights into the modeling of adsorption isotherm systems. Chem. Eng. J. 156 (1), 2–10.

Guo, X., Wang, J., 2019. A general kinetic model for adsorption: Theoretical analysis and modeling. J. Mol. Liq. 288, 111100.

Hames, B., Ruiz, R., Scarlata, C., Sluiter, A., Sluiter, J., Templeton, D., 2008. Preparation of samples for compositional analysis. National Renewable Energy Laboratory. NREL/TP-510-42620.

Hoang, A.T., Nguyen, X.P., Duong, X.Q., Ağbulut, Ü., Len, C., Nguyen, P.Q.P., Kchaou, M., Chen, W.-H., 2023. Steam explosion as sustainable biomass pretreatment technique for biofuel production: Characteristics and challenges. Bioresour. Technol. 385, 129398.

Ioannidou, O., Zabaniotou, A., 2007. Agricultural residues as precursors for activated carbon production—A review. Renew. Sustain. Energy Rev. 11 (9), 1966–2005.

Kant, R., 2012. Textile dyeing industry an environmental hazard. Nat. Sci. 4, 22–26.

Le Normand, M., Mélida, H., Holmbom, B.R., Michaelsen, T.E., Inngjerdingen, M., Bulone, V., Paulsen, B.S., Ek, M., 2014. Hot-water extracts from the inner bark of Norway spruce with immunomodulating activities. Carbohydr. Polym. 101, 699–704.

Lima, E.C., Ponce-Vargas, M., Naushad, M., Thue, P.S., dos Reis, G.S., Mello, B.L., Rabiee, N., Abatal, M., Korany Seliem, M., Badawi, M., 2024. Removal of methylparaben from aqueous effluents using biobased carbon material. Experimental and DFT calculations. J. Mol. Liq. 397, 124194.

Lin, S., Yu, J., Yao, A., Tian, S., Liao, H., Zhan, Y., Xiao, H., Lan, J., 2023. Mussel-inspired fabrication of pH-responsive pomelo peels as "smart" bio-based adsorbents for controllable removal of both cationic and anionic dyes. Sep. Purif. Technol. 326, 124744.

Malakootian, M., Heidari, M.R., 2018. Reactive orange 16 dye adsorption from aqueous solutions by psyllium seed powder as a low-cost biosorbent: kinetic and equilibrium studies. Appl Water Sci 8 (7), 212.

Marrakchi, F., Ahmed, M.J., Khanday, W.A., Asif, M., Hameed, B.H., 2017. Mesoporous carbonaceous material from fish scales as low-cost adsorbent for reactive orange 16 adsorption. J. Taiwan Inst. Chem. Eng. 71, 47–54.

Merlen, A., Buijnsters, J.G., Pardanaud, C., 2017. A guide to and review of the use of multiwavelength raman spectroscopy for characterizing defective aromatic carbon solids: from graphene to amorphous carbons. Coatings 7 (10), 153.

Muzamal, M., Jedvert, K., Theliander, H., Rasmuson, A., 2015. Structural changes in spruce wood during different steps of steam explosion pretreatment. Holzforschung 69.

Pimenta, M.A., Dresselhaus, G., Dresselhaus, M.S., Cançado, L.G., Jorio, A., Saito, R., 2007. Studying disorder in graphite-based systems by Raman spectroscopy. PCCP 9 (11), 1276–1290.

Pinheiro Nascimento, P.F., Barros Neto, E.L., 2021. Steam Explosion: Hydrothermal Pretreatment in the Production of an Adsorbent Material Using Coconut Husk. Bioenergy Res. 14 (1), 153–162.

Praveen, S., Jegan, J., Bhagavathi Pushpa, T., Gokulan, R., Bulgariu, L., 2022. Biochar for removal of dyes in contaminated water: an overview. Biochar 4 (1), 10.

Qasem, N.A.A., Mohammed, R.H., Lawal, D.U., 2021. Removal of heavy metal ions from wastewater: a comprehensive and critical review. npj Clean. Water 4 (1), 36.

Rosa, S., Laranjeira, M.C.M., Riela, H.G., Fávere, V.T., 2008. Cross-linked quaternary chitosan as an adsorbent for the removal of the reactive dye from aqueous solutions. J. Hazard. Mater. 155 (1), 253–260.

Sadezky, A., Muckenhuber, H., Grothe, H., Niessner, R., Pöschl, U., 2005. Raman microspectroscopy of soot and related carbonaceous materials: Spectral analysis and structural information. Carbon 43 (8), 1731–1742.

Sayed, N.S.M., Ahmed, A.S.A., Abdallah, M.H., Gouda, G.A., 2024. ZnO@ activated carbon derived from wood sawdust as adsorbent for removal of methyl red and methyl orange from aqueous solutions. Sci. Rep. 14 (1), 5384.

Shah, J.A., Butt, T.A., Mirza, C.R., Shaikh, A.J., Khan, M.S., Arshad, M., Riaz, N., Haroon, H., Gardazi, S.M.H., Yaqoob, K., Bilal, M., 2020. Phosphoric acid activated carbon from melia azedarach waste sawdust for adsorptive removal of reactive orange 16: equilibrium modelling and thermodynamic analysis. Molecules 25 (9), 2118.

Sluiter, A., Hames, B., Ruiz, R., Scarlata, C., Sluiter, J., Templeton, D., Crocker, D., 2008. Determinataion of Structural Carbohydrates and Lignin in Biomass. National Renewable Energy Laboratory. NREL/TP-510-42618.

Sutthasupa, S., Koo-amornpattana, W., Worasuwannarak, N., Prachakittikul, P., Teachawachirasiri, P., Wanthong, W., Thungthong, T., Inthapat, P., Chanamarn, W., Thawonbundit, C., Srifa, A., Ratchahat, S., Chaiwat, W., 2023. Sugarcane bagasse-derived granular activated carbon hybridized with ash in bio-based alginate/gelatin polymer matrix for methylene blue adsorption. Int. J. Biol. Macromol. 253, 127464.

Textile Exchange. 2022. Preferred Fiber & Materials Market Report.

Torget, R., Himmel, M.E., Grohmann, K., 1991. Dilute sulfuric acid pretreatment of hardwood bark. Bioresour. Technol. 35 (3), 239–246.

Vigneshwaran, S., Sirajudheen, P., Karthikeyan, P., Meenakshi, S., 2021. Fabrication of sulfur-doped biochar derived from tapioca peel waste with superior adsorption performance for the removal of Malachite green and Rhodamine B dyes. Surf. Interfaces 23, 100920.

Wang, J., Zhang, X., Li, Z., Ma, Y., Ma, L., 2020. Recent progress of biomass-derived carbon materials for supercapacitors. J. Power Sources 451, 227794.

Weber, W.J., Morris, J.C., 1963. Kinetics of adsorption on carbon from solution. J. Sanit. Eng. Div. 89 (2), 31–59.

Won, S.W., Choi, S.B., Yun, Y.-S., 2006. Performance and mechanism in binding of Reactive Orange 16 to various types of sludge. Biochem. Eng. J. 28 (2), 208–214.

Yang, Y., Cannon, F.S., 2021. Preparation of activated carbon from pine sawdust with hydrothermal-pressure preconditioning. J. Environ. Chem. Eng. 9 (6), 106391.

Yang, G., Pan, C., Yang, H., Feng, N., 2021. Carbon-supported nickel catalyst prepared from steam-exploded poplar by recovering Ni(II). BioResources 16, 5481–5493.

Yaseen, D.A., Scholz, M., 2019. Textile dye wastewater characteristics and constituents of synthetic effluents: a critical review. Int. J. Environ. Sci. Technol. 16 (2), 1193–1226.

Zhang, L., Liu, Z., Cui, G., Chen, L., 2015. Biomass-derived materials for electrochemical energy storages. Prog. Polym. Sci. 43, 136–164.